Electronic Supplementary Material (ESI) for Lab on a Chip.

Supplementary Information:

A Wearable Electrofluidic Actuation System

Haisong Lin[1†], Hannaneh Hojaiji[1†], Shuyu Lin[1†], Christopher Yeung[1,2], Yichao Zhao[1,2], Bo Wang[1], Meghana Malige[1], Yibo Wang[1], Kimber King[1], Wenzhuo Yu[1], Jiawei Tan[1,2], Zhaoqing Wang[1], Xuanbing Cheng[1,2], and Sam Emaminejad[1,3*]

[1] Interconnected & Integrated Bioelectronics Lab (I^2BL), Department of Electrical and Computer Engineering, University of California, Los Angeles, California

[2] Department of Materials Science and Engineering, University of California, Los Angeles, CA, USA

[3] Department of Bioengineering, University of California, Los Angeles, CA, USA

[†] These authors contributed equally to this work.

[*] Correspondence and requests for materials should be addressed to S.E. (emaminejad@ucla.edu)

Supplementary Methods

Device fabrication and assembly

To make the ACET electrodes amenable for wearable applications, the electrodes were patterned on a flexible PET substrate and incorporated into a tape-based flexible microfluidic device. The electrode fabrication followed the standard photolithography protocol, which included spin-coating and patterning a positive photoresist (MicroChemicals AZ5214E) layer, followed by the evaporation of Cr, Au, and Ti with thicknesses of 20 nm, 100 nm, and 20 nm, respectively. Lift-off was then performed in acetone. Next, the epidermal microfluidic device was created by assembling laser-cut layers of double-sided tape (170 μm-thick, 9474LE 300LSE, 3M), Skin adhesive medical tape (Tegaderm Transparent Film Dressing, 3M), bare PET (100 μm-thick, MG Chemicals), and PET patterned with the ACET electrodes. Laser-cutting was performed with the Epilog Mini 24 (Epilog Laser).

ACET Theory and Simulation

To investigate and model ACET-induced fluidic motion, finite element analysis (COMSOL Multiphysics 5.2) was used to perform electrothermal simulation. A comprehensive study on the simulation of electrothermal behavior of coplanar electrode pairs was previously presented by Meinhart et al. [1]. Given the similarity of our electrode and channel configurations, the same approach was adopted to simulate the ACET phenomena. In short, application of an AC voltage across a coplanar electrode pair establishes a non-uniform electric field and subsequently non-uniform temperature, permittivity, and conductivity profiles. Consequently, the interaction of the electric field and the charge density distribution (ρ) results in a non-zero body force on the fluid. In such a system, the charge distribution must satisfy both Gauss's law and the following charge conservation conditions (equations below):

$$\nabla \times E = 0 \quad (1)$$

$$\nabla \cdot (\varepsilon E) = \rho \quad (2)$$

$$\nabla \cdot (\sigma E) = -\frac{\partial \rho}{\partial t} \quad (3)$$

By solving the above equations in the frequency domain ($\partial/\partial t = i\omega$, where ω is the angular frequency of the excitation voltage), and by applying small permittivity and conductivity gradient approximations, the ρ can be expressed as [2]:

$$\rho = \nabla\varepsilon \cdot E_0 - \varepsilon_0 \frac{E_0 \cdot \nabla(\sigma + i\omega\varepsilon)}{\sigma_0 + i\omega\varepsilon_0} \quad (4)$$

, where the subscript 0 represents the variables for a spatially constant temperature T_0.

In the case of electrothermal kinetics, the temperature gradient-induced permittivity and conductivity gradients can be expressed as:

$$\nabla\varepsilon = \varepsilon_0\alpha\nabla T,\ \nabla\sigma = \sigma_0\beta\nabla T, \text{ where } \alpha = \frac{1}{\varepsilon}\frac{\partial\varepsilon}{\partial T},\ \beta = \frac{1}{\sigma}\frac{\partial\sigma}{\partial T} \quad (5)$$

, where for aqueous solutions at 25 ℃, $\alpha \approx -0.0046\ \mathrm{K}^{-1}$ and $\beta \approx 0.020\ \mathrm{K}^{-1}$ [3]. After calculating the space charge density, the electrical body force density can be determined, which is the sum of a Coulomb term and a dielectric term.

$$f = \rho E - \frac{1}{2}E^2\nabla\varepsilon \quad (6)$$

Combining (4), (5) and (6), the ACET body force can be expressed as:

$$f = \left[\frac{\varepsilon_0\sigma_0(\alpha-\beta)}{\sigma_0 + i\omega\varepsilon_0}\nabla T \cdot E_0\right]E_0 - \frac{1}{2}E_0^2\nabla\varepsilon \quad (7)$$

In the case of ACET biofluid actuation, conductivity and relative permittivity is 0.6 S/m and 80.2 respectively and AC frequency is 8 MHz. With $\omega \ll \sigma_0/\varepsilon_0$, low-frequency approximation can be applied and (7) can be simplified to:

$$f \approx -0.022\varepsilon_0 E_0^2\nabla T \quad (8)$$

which is defined as the body force in the Navier-Stokes equation when simulating laminar flow in the channel.

In the COMSOL Multiphysics simulation setup, laminar flow, heat transfer, and electric current physics were employed in the context of a 3D microfluidic channel (with a PET substrate and ceiling) containing a solution with properties similar to that of a biofluid (*e.g.*, sweat). The simulation used the same electrode dimensions as the experimental setup. The ceiling of the microfluidic channel was set as ambient temperature (25 ℃) and the bottom surface of the PET

substrate (assumed to be in direct contact with skin) was set as skin temperature. Other surfaces (walls of the channel) were assumed to be thermally insulated.

Mixing index calculation through image analysis

To quantify mixing efficiency, similar to previous efforts [4], the mixing of two side-by-side laminar flows (one 1X PBS, another 0.2X PBS dyed with Rhodamine B for visualization) was characterized under various excitation voltages and flow velocities. The microfluidic region containing the mixing electrode array was video-recorded, and the corresponding video frames were imported into Matlab (Mathworks). The boundaries of electrode pairs were identified by at the software level, and image analysis was performed at its neighboring region. Similar to previous work [4], a mixing index is defined, as expressed below, that calculates the reciprocal of the local dye density's standard deviation in the imaged region:

$$\text{Mixing index} = \frac{1}{s} = \sqrt{N / \sum_{i=1}^{N} (c_i - c_{ave})^2} \quad (9)$$

where N, c_i, and c_{ave} are the total number of pixels in the neighboring region, the intensity at pixel *i*, and the average intensity over *N* pixels, respectively. With this definition, a higher index value corresponds to a lower standard deviation, indicating greater dye density homogeneity in the imaged region. To normalize our readings, this index is linearly mapped over the range of 0 to 1, where 0 corresponds to the initial state with flow rate of 10 μL/min (negligible passive mixing), and 1 corresponds to the fully-mixed steady state where the whole image is homogeneous (e.g., at minute 3 of mixing for flow rate of 0.1μL/min).

Supplementary Figures

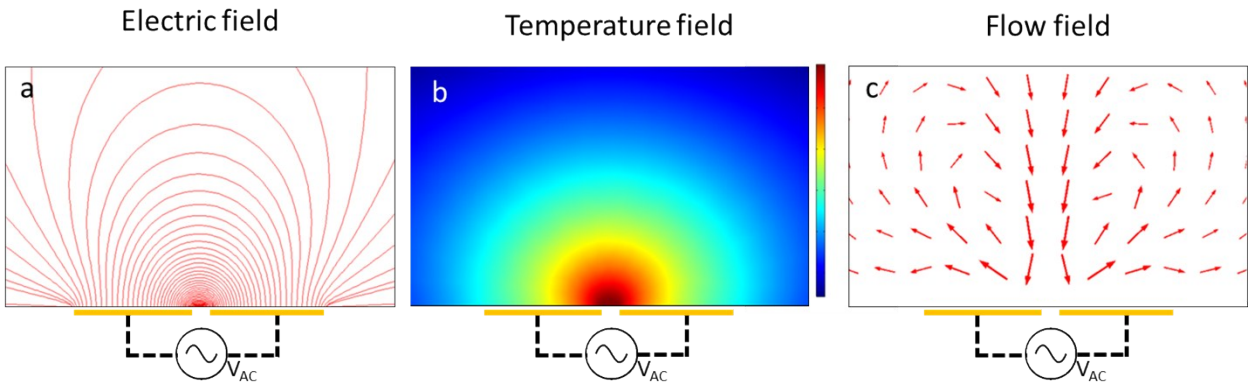

Fig. S1. Conceptual illustrations of the ACET-based electric field (a), temperature field (b), and flow field (c) profiles, generated by equally-sized coplanar pair of electrodes.

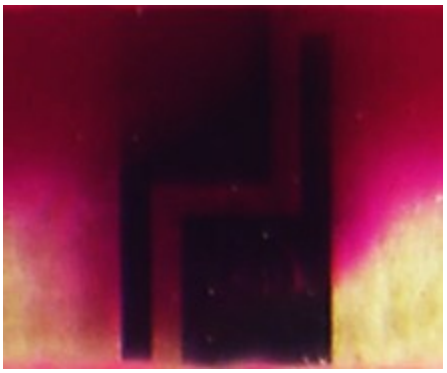

Fig. S2. Optical image of the intermittent stage of a mixing process showing that the strongest vortex occurs at the end junctions in-between the narrow and wide electrodes.

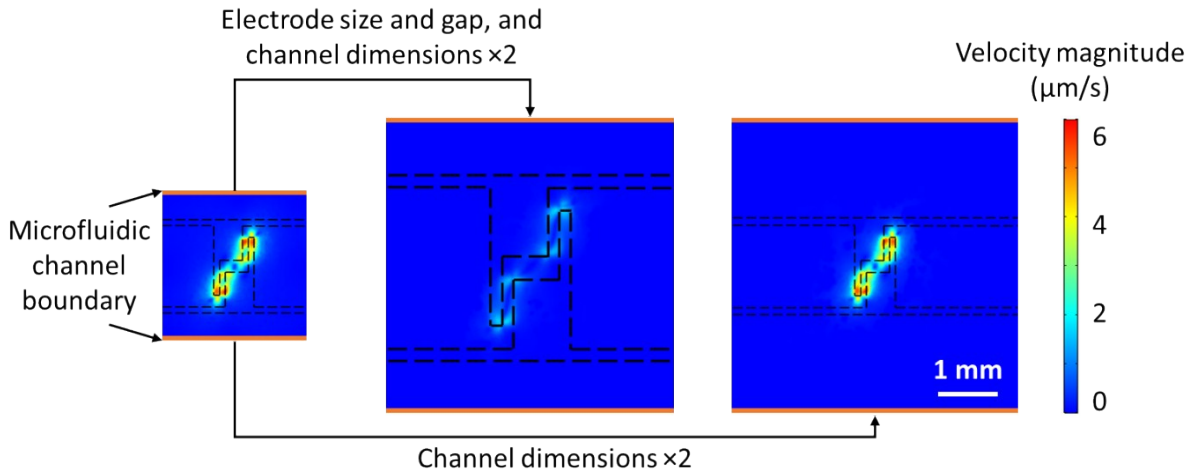

Fig. S3. Effect of device size scaling on ACET actuation. Simulated fluid velocity magnitude profiles of ACET mixing for three configurations (top view, microfluidic channel boundary defined by the brown line, at the 100 μm above the rotationally symmetric electrodes, applied voltage: 3.5 V_{rms}, fluid conductivity: 0.6 S/m): 1) original design (left, discussed in the main text, Fig. 3), 2) design with electrode size and gap, and channel dimensions ×2 (center), and 3) design with channel dimensions ×2 only (right). Comparison of the results of the configurations 1 and 2 yields that the increased scaling of the dimensions leads to a substantial decrease in the ACET-induced velocities (because of the reduction in electric field magnitude). Comparison of the results of the configurations 1 and 3 yields that the increased scaling of the channel (without scaling the electrode dimensions) leads to negligible decrease in the ACET-induced velocities (because the electric field concentrated region between the two electrodes is minimally affected).

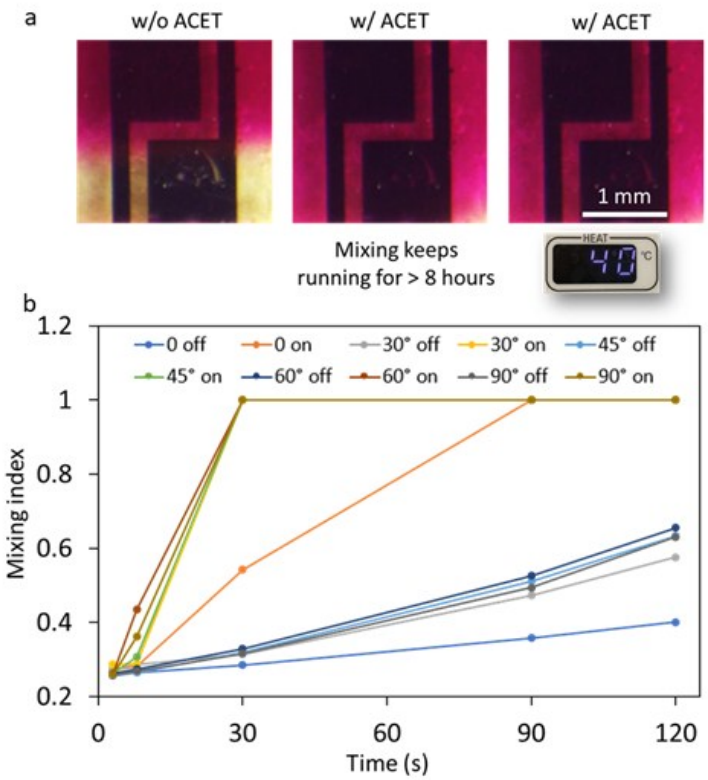

Fig. S4. Stability of ACET actuation. a) Optical images of the ACET mixing process when ACET actuation was deactivated, activated for more than 8 hrs at room temperature, and activated with a surrounding temperature of 40 ^{o}C. b) Mixing index vs. time for various device orientations (externally driven flow rate: 0.5 µL/min, ACET Voltage: 3.5 V_{rms}).

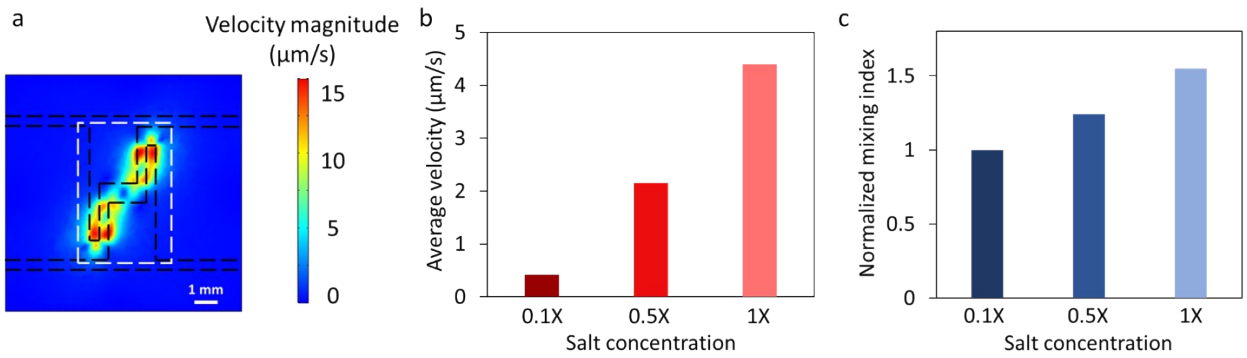

Fig. S5. Influence of the solution salt concentration on ACET actuation. a) Simulated fluid velocity magnitude profile (top view, at the 100 μm above the rotationally symmetric electrodes, applied voltage: 3.5 V_{rms}, fluid conductivity: 1.6 S/m). The white box outlines the area analyzed in Fig. S5b. b) Simulated velocity magnitude with different salt concentration levels (averaged over the outlined area in Fig. S5a, assumed fluid conductivity values of 0.16, 0.8, 1.6 S/m for 0.1X, 0.5X and 1X PBS solutions, respectively). c) Experimentally characterized mixing index vs. solution salt concentration level (normalized with respect to the 0.1X PBS solution case).

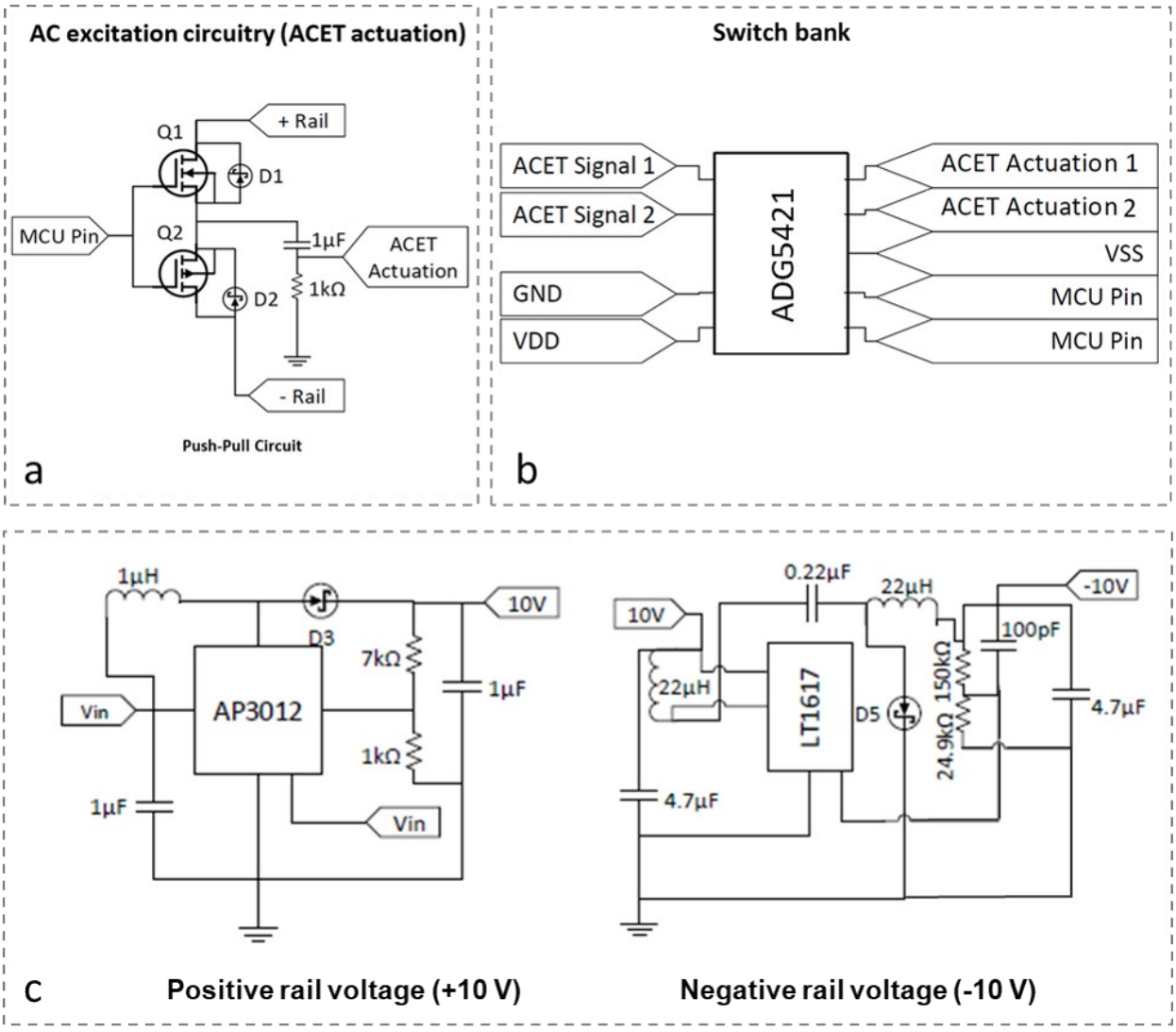

Fig. S6. Overview of the wireless FPCB. Schematic diagram of the a) AC excitation circuit (including the peripheral components). b) ACET switching circuit (implementing a two-channel activation and actuation). c) Implementation of the positive and negative rails of the push-pull circuit using AP3012 (SOT-23-5 – Diodes Inc.) and LT 1617 (SOT-23 – Linear Technology) integrated circuit chips to generate +10 V and -10 V.

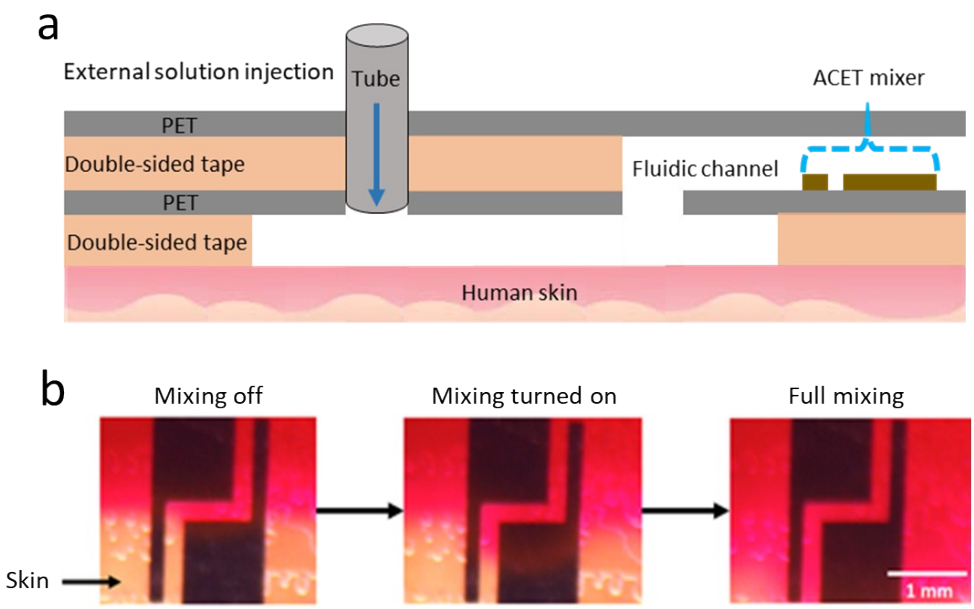

Fig. S7. Visualization of the ACET actuation with the wireless electrofluidic actuation system, performed on body with externally-pumped model solutions (1X transparent and 0.2X red-dyed PBS solutions). a) Cross-view schematic of the device-epidermal interface (for the channel containing the transparent solution). b) Sequential optical images of the on-body mixing process. For the channel containing the red-dyed solution, a PET layer is used, to physically isolate the solution from the skin.

Table S1. Power consumption *vs.* Mixing index for different ACET excitation voltage levels (performed in 1X PBS solution, excited by a function generator Tektronix AFG3102C).

Voltage (V_{rms})	Power (mW)	Mixing index
0.9	0.03	0.11
1.8	0.275	0.14
2.7	0.99	0.26
3.5	2.35	0.48

References

1. S. Loire, P. Kauffmann, I. Mezić and C. D. Meinhart, *Journal of Physics D: Applied Physics*, 2012, 45, 185301.
2. A. González, A. Ramos, H. Morgan, N. G. Green and A. Castellanos, Journal of Fluid Mechanics, 2006, 564, 415.
3. C. D. Hodgman and S. C. Lind, The Journal of Physical and Colloid Chemistry, 1949, 53, 1139–1139.
4. H.-Y. Wu and C.-H. Liu, *Sensors and Actuators A: Physical*, 2005, 118, 107–115.